Rapid reduction in the shear resistance and permeability of soft interlayers within a limited shear displacement under water weathering

Guoqing Chen*[1]; Tao Wei[1]; Lei Wu[1]; Fangzhou Liu[2]

1. State Key Laboratory of Geohazard Prevention and Geoenvironment Protection, Chengdu University of Technology, Chengdu, China; *2. Department of Civil and Environment Engineering, University of Alberta, Edmonton, Canada*

Abstract: The activation of landslides and shallow faults is related to the shear behavior of soft interlayers during groundwater infiltration. Regarding the water sensitivity of clay minerals, the shear behavior of soft interlayers may rely more on weathering and water content than the requirement of shear displacement and normal stress for quartz grains. Here, we present the reduction characteristics of the shear resistance and permeability of mudstone granules considering weathering under dry-wet cycling. Within a shear displacement of 20 mm, the shear mode transformation of the weathered mudstone granules from strain hardening to strain softening was revealed from dry to wet conditions. However, this transition was not observed for unweathered mudstone and weathered sandstone samples. Correspondingly, the permeability perpendicular to the shear zone reduced 10~45 times with increasing normal stress according to post-shear measurements. Because weathered particles exhibited more micropores, the addition of water resulted in mineral separation and generated mud that filled the specimen pores. Thus, the sealing and lubrication effect of the mud decreased the porosity and shear resistance of the soft interlayer, along with increasing particle roundness. This rapid transformation mechanism within a limited displacement reveals the effect of water softening and weathering on the shear behavior of soft interlayers, which helps to understand landslide occurrence and shallow fault activation.

Key words: Weathered soft interlayer; mudstone granules; shear behavior; permeability; dry-wet cycle.

Plain language summary

The shear strength and shear-induced permeability variation of soft interlayers are significant for occurrence of landslide and activation of shallow fault. Their properties are related to the shear rate and displacement, effective normal stress and water content, particle size distribution and mineral composition. Different from the hard grains as quartz, the sensitivity of mudstone to water induces the layered rock mass fracturing and softening into finer fragments. Although with a wide range of particle size distribution, rapid reduction of shear strength and permeability for the soft interlayer when encountered water has triggered catastrophic landslides disaster. How this softening behavior happening is practical significance. Here, we present that the weathered mudstone granules tend to transform into mud in wet conditions due to the increment of micropore after long-term weathering of water. Within a limited shear displacement, wet granules could trigger the reduction of shear strength and permeability, which

deepens our understanding of soft interlayers in slope stability and fault activation when groundwater infiltrates.

1 Introduction

The development of soft interlayers in sandwich strata and fault gouges is a crucial geological structure related to landslide and shallow fault activation (Christaras, 1997; Eberhardt et al., 2005; Ma et al., 2019; Panek et al., 2011; Zou et al., 2017). Extensive slope failure cases in southwest China (Li et al., 2020; Tang et al., 2015; Xu et al., 2016) and other regions of the world (Christaras, 1997; Eberhardt et al., 2005; Panek et al., 2011) have been observed to be controlled by a argillic soft interlayer. Smectite-clay gouge and mudstone are widely found at different depths in fault zone (Cuisiat and Skurtveit, 2010; Ikari et al., 2009; Morrow et al., 2015). In general, the shear band crushing induced low resistance was relevant to the particle shape and size distribution (Feia et al., 2016; Mair et al., 2002), lithology, water content (Crawford et al., 2008; Ma et al., 2019; Zhang et al., 1999), shear speed and effective normal stress (Fukuoka et al., 2007; Kimura et al., 2018; Lupini et al., 1981). In ring shear tests, samples of hard grains required a large displacement and high normal stress to reach their residual strengths (Fukuoka et al., 2007; Kimura et al., 2019). For a soft interlayer consisting of clay grains, Ma et al. (2019) revealed the dependency of the transformation from strain hardening to strain softening on the water content. Due to the sensitivity of clay minerals to water, the shear behavior of mudstone granules considering the effect of weathering is of engineering significance (Chandler, 1969). Thus, different in sensibility to weathering between clay minerals and quartz, the relationships of the shear behavior of mudstone granules to shear conditions, such as the water content, shear displacement, and normal stress, have remained enigmatic when considering the influence of water weathering.

The shear-induced reduction in permeability contributed by crushing band with a few millimeters thickness has been studied through particle size analysis, high-speed imaging, and field emission scanning electron microscopy (Agung et al., 2004; Cuisiat and Skurtveit, 2010; Fukuoka et al., 2007; Kimura et al., 2019; Kimura et al., 2020; Kimura et al., 2018). The ring shear test results (Kimura et al., 2020; Kimura et al., 2018) demonstrate the negative effect of shear rate and effective normal stress (within 10 MPa) on silica sand permeability. However, the permeability of fault gouges under tens of megapascals of normal stress has no significant relationship with shear speed (Tanikawa et al., 2012). At the microscale, blockage of the pore throat by fine particles and rearrangement of the flaky minerals was attributed to the variation in effective porosity and permeability (Dewhurst et al., 1996; Schneider et al., 2011; Zhang et al., 1999). Although the permeability reduction property of quartz grains after shearing explains the fluid distribution of faults and sealing properties of sediment (Kimura et al., 2019; Tanikawa et al., 2012), it seems difficult to extend to soft interlay-

ers composed of clay rock due to their distinct mineralogy and shear behavior (Crawford et al., 2008; Ma et al., 2019; Zhang et al., 1999).

Thus, mudstone granules from red sandwich strata in a landslide were prepared to research the shear behavior and permeability of soft interlayers under different weathering intensities through dry-wet cycling. To clarify the weathering effect on the specimens, the change in particle shape and formation of micropores with dry-wet cycle was discussed in terms of their influence on shear behavior and permeability. The results suggested that the increment of particle micropore promoted clay mineral separation and transformation into mud, which filled the specimen pores, inducing a rapid reduction in the shear resistance and permeability of the soft interlayer.

2 Materials and methods

2.1 Sample description and preparation

The tested samples were collected from the Wujiafen (WJF) landslide, which was located at Zhuanfang village, eastern Chengdu Hi-Tech Industrial Development Zone, Sichuan Provence, China. Similar to the Leidashi (LDS) landslide in its 10° north by east about 2 km long. The WJF landslide collapsed along a gently inclined bedding plane due to heavy rainfall in August 2019 (Li et al., 2020). As the field investigation showed (Fig. 1), a sandwich rock structure consisting of red mudstone and argillaceous sandstone of the Triassic Penglaizhen Formation was revealed in the left lateral scarp of the WJF landslide. Intact mudstone and sandstone with slight weathering were sampled by avoiding a soft interlayer (pressed in by the cutting ring) that was parallel to the sliding direction. The physical and mechanical properties of the rock samples in Table 1 were determined in laboratory tests.

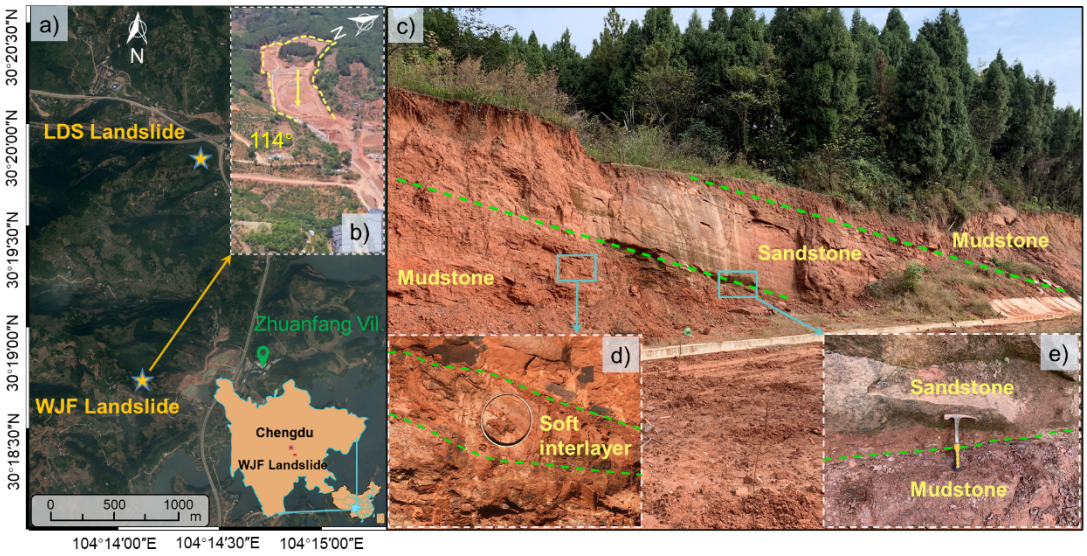

Fig. 1 Locations of the a) and b) WJF landslide and c) sampling site. d) Soft interlayer in the mudstone. e) Sandwich structure of the sandstone and mudstone.

Table 1 Physical and mechanical properties of the rock samples

Rock type	Dry density /(g · cm^{-3}	Natural water content/%	Void ratio /%	Uniaxial compressive strength (MPa)	
				Dry	Natural
Mudstone				~20.8	~14.9
Sandstone				~25.8	~23.3

Given the durability of mudstone and the sensitivity of clay minerals to water (Liu et al., 2020), dry-wet cycling of the specimens was carried out to consider the water variation in the rock mass with seasonal and environmental temperature changes (Gokceoglu et al., 2000; Zhang and Gao, 2020). The samples were crushed into 2~5 mm grains, dried at 40°C for four days, sprayed with water (15% of the granule mass) and maintained in a sealed bucket for eight days. After each dry-wet cycle, granule samples were sieved to pass a 2 mm sifter to prepare coarse granules for next cycle. Sandstone grains were also tested to discuss the difference of weathering to lithology. The granule samples were labeled by cycle number, as shown in Fig. 2, where the samples before dry-wet cycling and after the 3rd and 6th dry-wet cycles were categorized into unweathered and

weathered states, respectively.

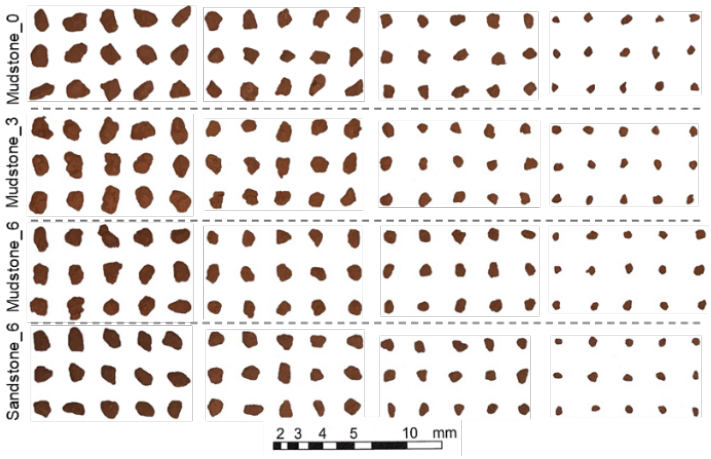

Fig. 2 Granules used in this study through crushing and dry-wet cycles

2.2 Test setup for limited shear displacement

The progress and development of ring shear apparatuses have provided an effective approach for exploring the dynamic shear process of quartz granules under large shear displacement and high normal stress conditions (Fukuoka et al., 2007; Kimura et al., 2019; Mair et al., 2002; Tanikawa et al., 2012). Due to the difference in lithology between mudstone and quartz, the shear behavior of soft interlayers may rely more on the water content and weathering intensity rather than the shear displacement and normal stress. To select appropriate shear box dimensions, ASTM D 3080 (2001) suggests a minimum specimen width of at least 10 times the maximum particle size diameter, a minimum width-to-thickness ratio of 2, and a minimum initial specimen thickness of six times the maximum particle diameter. With a maximum particle size of 5 mm, a self-developed digital direct shear test apparatus (shear box dimensions of 200*200*200 mm^3) was used in this study; the bottom of the shear box was filled with quartz grains 2~5 mm in size to ensure that the sheared samples were 40 mm thick. Two digital force sensors were equipped in the vertical and horizontal directions, and the shear and normal forces were loaded with a hydraulic system. With this system, the shearing rate can be controlled in the range of 0.05~10 mm/s.

Considering the strength reduction of mudstone under the action of water, normal stresses ranging from 200 kPa to 1400 kPa were adopted in the direct shear tests with a constant shear speed of 0.1 mm/s until a shear displacement of 20 mm was reached. The highest normal stress of each group decreased with increasing dry-wet cycle number. Two conditions, dry and wet (water content equal to 15% of the dry specimen mass), were introduced to discuss the attenuation behavior of strength due to water.

2.3 Testing procedure

Each specimen was filled in the shear box in three equal layers, each subjected to 25 blows with a light compactor (2.5 kg hand rammer falling from 305 mm) to preset the target dry density of 1.337 g/cm^3. The top of each layer was loosened before the next filling and compaction to keep the sample homogeneous. The prespecified normal stress was applied to consolidate the specimen until the vertical displacement was constant. After reaching the preset shear displacement, the cutting ring (with a 61.8 mm diameter and 40 mm height) was gently pushed into the sheared specimen from a vertical direction to measure the permeability with the TST-55 falling-head permeameter.

To analyze the variation in particle shape with dry-wet cycles, PCAS software (Liu et al., 2011) was adopted to obtain the shape coefficients by statistically analyzing 480 particles with different sizes. Five coefficients were taken into analysis, including the uniformity coefficient (UC), sorting coefficient (SC), curvature coefficient (CC), average form factor (AFF), and fractal dimension (FD). Coarse granules were broken to obtain the cross-section for observing their microstructure in Thermo Scientific Prisma E environmental scanning electron microscope (ESEM).

3 Results

3.1 Shear resistance

The direct shear results shown in Fig. 3 demonstrate that the peak shear stress of mudstone granules decreased with an increasing number of dry-wet cycles when tested under both dry and wet conditions. Notably, the variation in the original direct shear data was smoothed with the fast Fourier transform method. Strain hardening behavior was observed for the dry specimens: the shear stress increased rapidly and remained constant near the peak strength without significantly decreasing with increasing shear displacement. Although a wide normal stress range from 200 kPa to 1400 kPa was applied, dependance of the strain softening behavior on the normal stress observed in Ma et al. (2019) was not revealed within 20 mm of shear displacement. With increasing weathering intensity, the drop in the peak shear stress of the dry specimens increased at a higher normal stress. Compared with the mudstone, the sandstone exhibited a greater reduction in the peak shear stress between different normal stresses in the strain hardening curves after 6 dry-wet cycles (Fig. 3 d).

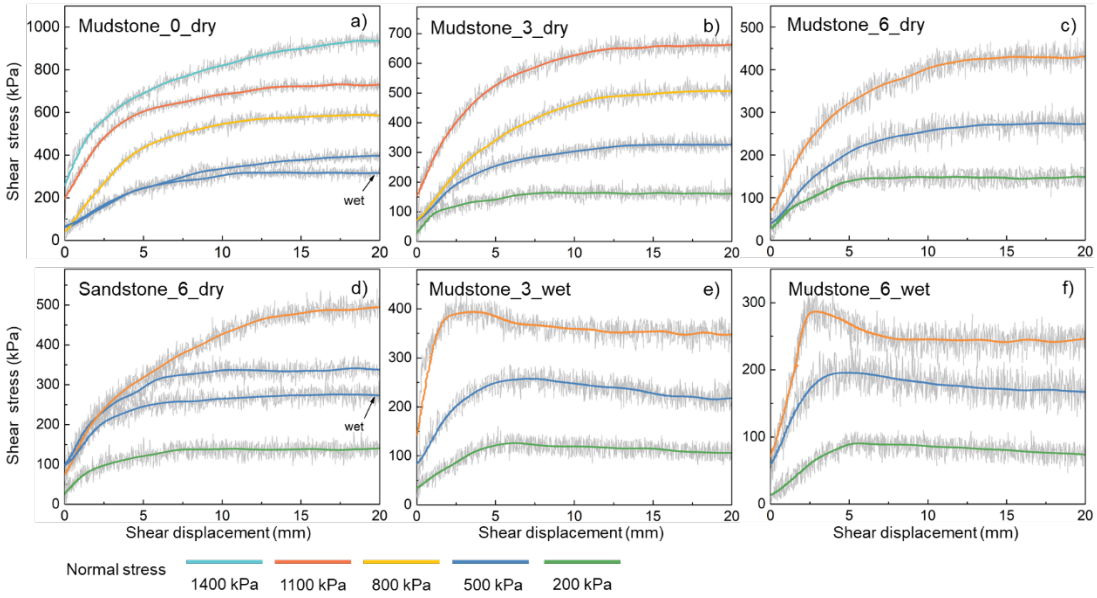

Fig. 3 Shear displacement-shear stress curves under different conditions. a) Mudstone granules sheared in both dry and wet conditions after 0 dry-wet cycles; b) and e) mudstone granules sheared in dry conditions and wet conditions after 3 dry-wet cycles, respectively; c) and f) mudstone granules sheared in dry conditions and wet conditions after 6 dry-wet cycles, respectively; d) sandstone granules sheared in both dry and wet conditions after 6 dry-wet cycles.

When the granules encountered water, the shear mode of the weathered mudstone samples changed from strain hardening to strain softening (Fig. 2 b vs. Fig. 2 e and Fig. 2 c vs. Fig. 2 f). A higher normal stress led to a greater difference between the peak and residual shear stresses for mudstone_3 and mudstone_6. In contrast, the same strain hardening behavior was observed for wet mudstone_0 and sandstone_6 under 500 kPa of normal stress. This indicated that the attenuation of the rock response due to water induced only a shear stress reduction and not further crushing to reach the residual strength. The difference in the shear stress reduction suggested that the weathering intensity was enhanced with an increasing number of the dry-wet cycles.

According to the Mohr-Coulomb yielding criteria, the cohesion (c) and internal friction angle ( ) of the peak strength and residual strength were analyzed (Fig. 4). The reduction in cohesion at the peak strength (c_{pd}) was dramatic in the dry condition once the mudstone granules underwent dry-wet cycling. A further reduction in cohesion between mudstone_3 and mudstone_6 was found in the wet condition (c_{pw}). In comparison to the cohesion, the internal friction angle decreased from mudstone_0 to mudstone_3 by approximately 1° and 6° in the dry and wet conditions, respectively, while the corresponding results were 5° and 12° for mudstone_6. In the residual stage, the residual internal friction angle

($_{rw}$) continued to drop with the dry-wet cycles, while the residual cohesion (c_{rw}) remained constant. In addition, the difference in shear strength between the mudstone and sandstone could be attributed to the lithology, as sandstone minerals are harder than clay minerals but lack interparticle cohesion in the crushed state.

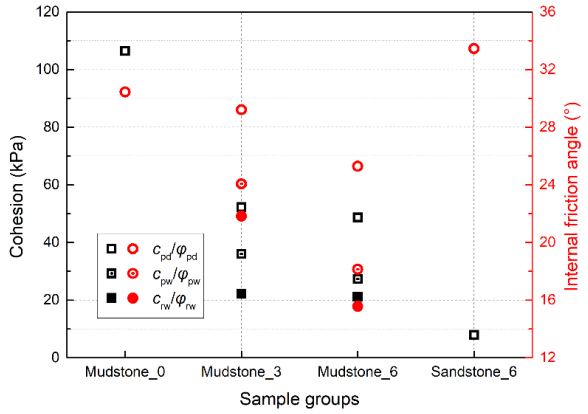

Fig. 4 Shear strength parameters (cohesion c and internal friction angle) of the four kinds of samples. Note: $c_{pd}/$ $_{pd}$ represents c and at the peak strength of dry samples. $c_{pw}/$ $_{pw}$ represents c and at the peak strength of wet samples. $c_{rw}/$ $_{rw}$ represents c and at the residual strength of wet samples.

3.2 Permeability of sheared specimens

The permeability coefficient of the sheared specimen in Fig. 5 revealed negative correlations between the permeability and normal stress, and the permeability and number of dry-wet cycles. A linear reduction in the permeability coefficient with increasing normal stress was found for all the mudstone specimens, although the weathered specimens in dry conditions presented a considerable fluctuation, which may be attributed to the heterogeneity of particles. Under the softening impact of water, the permeability coefficient of weathered mudstone granules decreased sharply with increasing normal stress when compared to the results of mudstone_0 and was close to 1.0×10^{-5} cm/s. The permeability difference between the dry and wet conditions of the weathered samples varied from 10 to 45 times with increasing normal stress at a limited shear displacement of 20 mm. Under the wet condition, a small reduction in the permeability of mudstone_0 was observed, but its permeability was still lower than that of most dry specimens. By fitting the data in a linear relation, the reduction in the slope from dry to wet conditions demonstrated that the change in permeability induced by the increasing normal stress was decreasing. The influence of weathering intensity on permeability was lower for mudstone_3 and mudstone_6 because of the decreasing discrepancy under wet conditions, while this

trend was not apparent in dry conditions. Due to the low cohesion of the samples, the permeability of the sandstone was higher than that of the mudstone, so it was more difficult to obtain the mudstone results under the same test conditions. Thus, the difference in the permeability coefficient controlled by lithology was not discussed in this study.

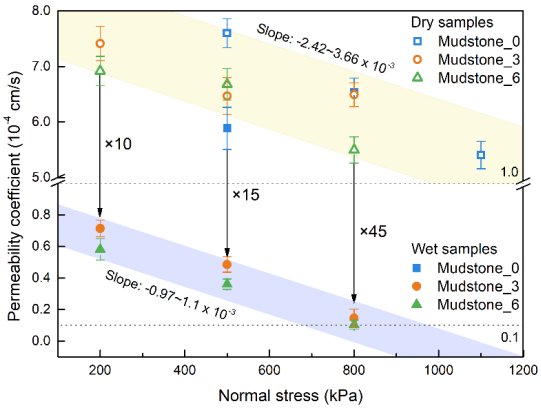

Fig. 5 Permeability coefficient of the sheared specimen under different normal stresses.

As shown in the cross-sections of the sheared specimen in Fig. 6, a visual distinction between the dry and wet samples was observed, where mudstone_3 presented more interparticle pores than mudstone_6. Although the crushing character of the shear band was found in the particle size distribution, where the content of the 2~1 mm grain size in the middle of the specimen was higher than those in the upper and lower parts. The dry specimen showed limited fragmentation under shearing and compression, which was reflected in the absence of a thin crushing zone after the ring shear tests (Fukuoka et al., 2007; Kimura et al., 2018). Therefore, the confined water could flow through the macropores and across the shearing zone easily. In contrast, the macropores of the wet specimen were filled with mud and almost disappeared. The particle content finer than 2~5 mm was increased throughout the specimen of mudstone_6 under wet conditions and a normal stress of 800 kPa. Similarly, extensive crushing in the middle part of mudstone_6 was revealed via the further increase of finer particle content, resulting in the strain softening behavior of weathered mudstone granules under wet conditions. The difference in the finer particle content between the dry and wet conditions supported the variation in the macropores observed in the cross-sections.

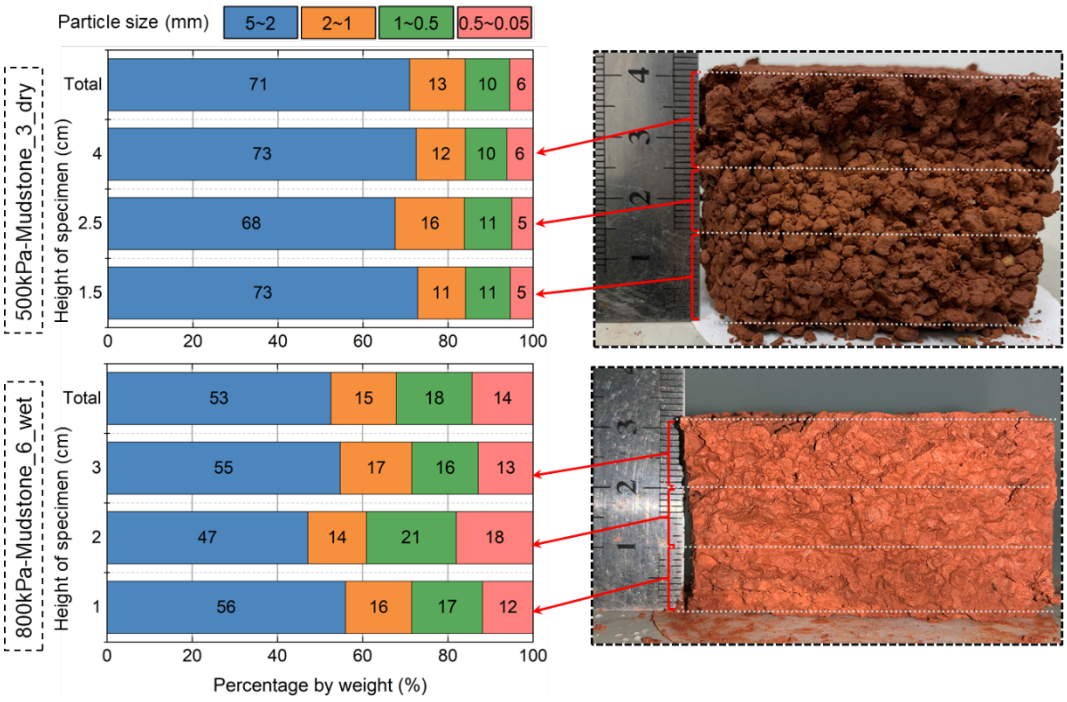

Fig. 6 Particle size distributions of a sheared specimen (left) corresponding to each layer of a cross-section (right).

3.3 Micropore increases for the weathered mudstone granules

The ESEM images in Fig. 7 suggest that the microstructure of the mudstone samples varied with the number of dry-wet cycles. At low magnifications (200 m and 500 m), mudstone_0 had no significant microstructure at the particle boundaries, which was the same as that observed in the interior of the particles. The mineral arrangement was relatively consistent according to the homogeneous grayscale, indicating a lower surface roughness for mudstone_0 than for the weathered particles. After the dry-wet cycling treatment, several micropores of approximately 80 m were found at the particle boundaries in mudstone_3. Many more micropores (approximately 50~300 m) were observed from the boundary to the inside of the particles in mudstone_6, due to the further development of water-rock interactions. Analogously, at the high magnification (mineral scale), there was almost an absence of cracks and micropores in mudstone_0, while the direction of mineral arrangement was fairly consistent. This kind of homogeneity demonstrated that the mudstone samples without dry-wet treatment were undamaged. On the other hand, the mineral distribution of the weathered granules was disordered, resulting in a higher roughness than that observed for mudstone_0. Thus, the damage feature from the boundary to

the inside of particles may be based on the micropore evolution process during dry-wet cycling (Fig. 7).

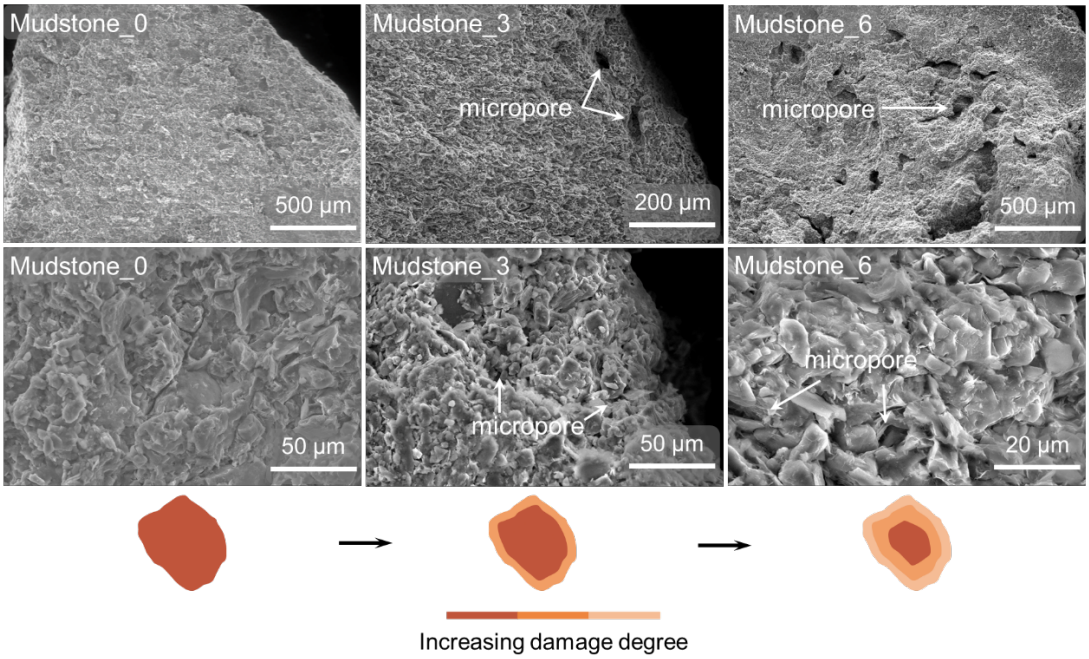

Fig. 7 Variation in the microstructure of the mudstone particles with an increasing number of dry-wet cycles at different magnifications. The sketch at the bottom describes the damage degree related to the variation in microstructure.

3.4 Variation in the granule shapes

Here, the shape coefficient results for the entire 2~5 mm particle size range are shown in Fig. 8. Compared to mudstone_0, the weathered mudstone granules exhibited a distinct variation phenomenon regardless of the reduction or increment in the four coefficients. Regarding the grain size composition, the UC and SC dropped continuously to approach 1.0, which indicated a better uniformity and sorting when the mudstone granules underwent dry-wet cycling. The four groups of specimens had no distinct difference in the CC, which fluctuated around the value of 1.05. The FD describes the autocorrelation of the change rate of the perimeter (c) in response to the change in area (S), which can be simplified as

where a is constant. The increase in the FD for weathered specimens, both mudstone and sandstone, indicated a strong correlation between perimeter and area. A slight change in area could induce a considerable variation in the perimeter for a higher FD. Another coefficient expressing the relationship between the

particle perimeter and area, the AFF, increased with the number of dry-wet cycles and approached 1.0, which corresponds to the maximum value for the circle. Therefore, the complexity of the mudstone particle boundaries decreased with area variation. It can be deduced that the shapes of the mudstone granules tended to change from polygons to circles with further weathering via dry-wet cycling, increasing the uniformity of the particle size distribution. In addition, among the four specimens, the sandstone exhibited generally low values of UC, SC, CC, and FD but the highest AFF. This difference can be attributed to the lower boundary of fracture surface complexity and better resistance to weathering of sandstone under dry-wet cycling.

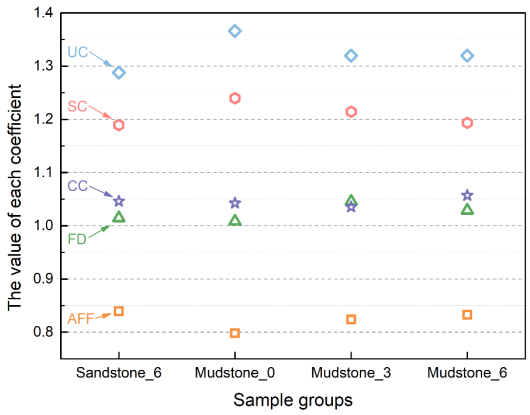

Fig. 8 Particle shape coefficients analyzed by PCAS software for the different lithologies and weathering intensities tested.

4 Discussion and mechanism analysis

4.1 Mechanism of the shear mode variation

The transformation of the shear mode of a granular specimen is important to describe the shear mechanism of a soft interlayer; in our results, this transformation was influenced by the weathering intensity and water condition. No significant residual strength was revealed for mudstone_0 or other specimens under dry conditions, which was similar to the ring shear results of soft interlayers at low water contents or high normal stresses obtained by Ma et al. (2019). The strain hardening of weathered specimens suggested that the crushing of particles was insufficient with limited shear displacement and concentrated in the middle part of the specimens, as shown in Fig. 6. The results of Alberti et al. (2019), Fukuoka et al. (2007) and Riaz et al. (2019) suggested that the shear resistance of quartz grains is almost constant in the initial stage, within a small displacement. Cuisiat and Skurtveit (2010) stated that the similar strain

hardening behaviors of layered sand and clay in the normal stress of 0.7 MPa. Thus, the dry specimens showed a shear behavior similar to that of specimens of quartz grains, with no apparent dependency on the normal stress within a limited shear displacement (Agung et al., 2004; Faoro et al., 2009; Fukuoka et al., 2007; Kimura et al., 2020; Mair et al., 2002; Tanikawa et al., 2012). According to the description of the turbulent mode in residual shear presented by Lupini et al. (1981), particles slide along the contact surfaces, which induced the damaged part of weathered particle crushing into debris under both shear and compression (Fig. 9 a). With a limited shear displacement, the debris with a strength equal to that of the rock is not crushed enough to attain a residual strength in dry conditions.

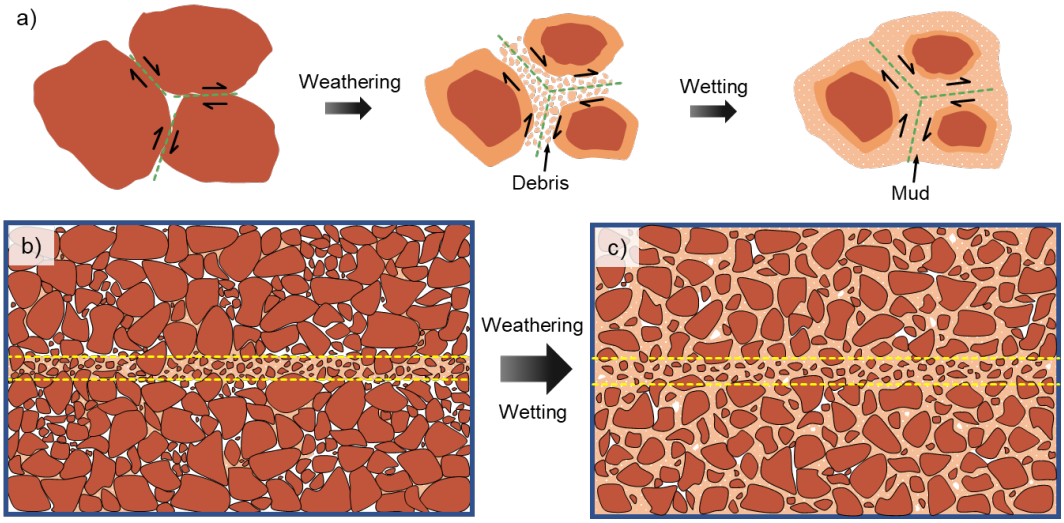

Fig. 9 Shear mode and variation in permeability of mudstone granules in the process of weathering and wetting. a) Variation in the shear mode with the action of weathering and wetting. b) Dry specimen containing debris in the shear band. c) Weathered mudstone granules changed changing into mud when encountering water.

As shown in Fig. 6 and Fig. 10, the fine particle contents were different between the weathered and unweathered samples and between the dry and wet conditions. According to the ESEM images, the loose parts of the particle boundaries tend to separate the clay minerals from each other and transform them into mud when exposed to water (Fig. 9 a). Therefore, mud wrapped the particles and served as lubrication, which obviously decreased the shear resistance more than the debris generated under dry conditions. This facilitated the shear behavior of granular specimens transitioning into strain softening within a limited shear displacement. Thus, the softening effect of water on the damaged part decreased the requirement of a large shear displacement to reach the residual strength. Although the role of water was considered in many hard particle shear tests

(Agung et al., 2004; Fukuoka et al., 2007), the water provided interparticle lubrication or bore the pore pressure rather than induced strain softening of the particles. Therefore, the strain softening behavior of the soft interlayer was closely connected to the combination of the water softening and weathering intensity to the mudstone grains (Chandler, 1969; Ma et al., 2019). Moreover, the roundness and uniformity of the granules increased with the weathering intensity, which corresponded to the low friction mechanism presented by Mair et al. (2002), who found that spherical glass beads show a lower resistance than angular quartz grains do when no particle crushing occurs.

4.2 Rapid reduction in the permeability

The permeability of the loose medium was controlled by the void ratio, which can vary with the particle size distribution and mineralogy, confining stress, shear displacement, and flow path (Crawford et al., 2008; Dewhurst et al., 1996; Faoro et al., 2009; Feia et al., 2016; Ikari and Saffer, 2012; Kimura et al., 2019; Reece et al., 2012; Zhang et al., 1999). From the dry condition to the wet condition, an increasingly strong relationship between the finer particle content and the normal stress after shearing was found, as shown in Fig. 10, which was verified in other studies (Feia et al., 2016; Kimura et al., 2020; Tanikawa et al., 2012). Regarding the differences in the permeability and finer particle content between the dry and wet samples, apparent crushing in the shear band occurred after the peak stress or a large shear displacement (Ikari and Saffer, 2012; Kimura et al., 2018; Uehara and Takahashi, 2014). More importantly, although these differences were also found for fault gouges with clay components (Tanikawa et al., 2012), there was a lack of discussion of the relationship between the increase in weathering intensity and finer particle generation, where our results showed a positive relationship (Fig. 10). With the increasing content of clay in the fault gauge, the permeability reduction was more prominent than that observed for quartz grains within a small shear strain (Crawford et al., 2008). Therefore, the permeability of the soft interlayer after shearing was closely related to the weathering intensity and water content within a limited shear displacement. Different from the crushing behavior concentrated in the shear band observed among the hard grains (Fukuoka et al., 2007), the weathered particles tended to transform into mud and fill the pores of the entire specimen under wet conditions, as described in Fig. 9 c and d. Mud blocking of the pore throats not only decreased the macropore content but also increased the compactness, so the vertical height of the wet specimens were greater than those of the corresponding dry specimens in Fig. 6. Similar to the results of the particle size distribution analysis in Fig. 6, more finer particles were found along the two sides of the shear bands in the weathered specimens under wet conditions. Thus, the variation in the permeability of the sheared soft interlayer was not only controlled by shear crushing in the shear band but also influenced by the argillization of the whole specimen. In addition, the permeability anisotropy between the directions parallel and perpendicular to the shear band was attributed to the difference in the finer particle distributions and rearrangement of clay minerals (Dewhurst

et al., 1996; Zhang et al., 1999). Correspondingly, the slight variation in our results of the finer particle content in the vertical direction complicates this anisotropy, which is worthy of further investigation in future work.

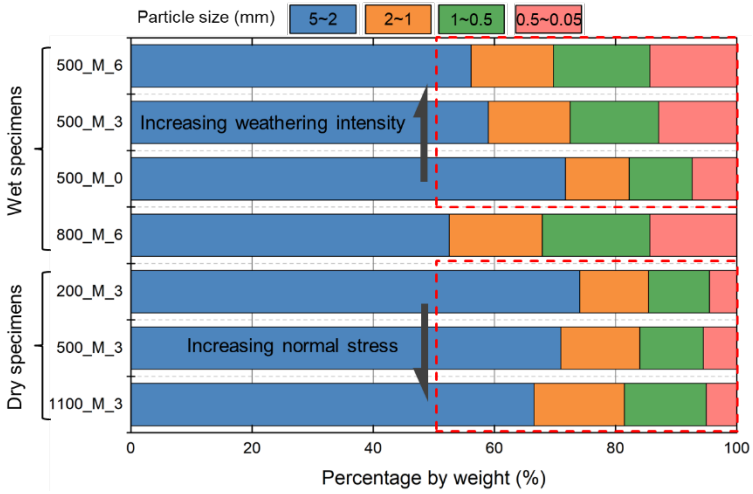

Fig. 10 Particle size distribution after 20 mm of shear displacement to evaluate the impact of weathering intensity and normal stress on the crushing degree of specimens. Note: For example, the label 500_M_3 means that the corresponding mudstone samples were sheared under 500 kPa of normal stress after 3 dry-wet cycles.

5 Conclusion

This study determined the rapid reductions in shear resistance and permeability of soft interlayers within a limited shear displacement of 20 mm. A weak dependency of the strain softening behavior on the normal stress was found for dry mudstone granules. Under wet conditions, the shear mode transformed from strain hardening to strain softening for weathered mudstone granules within a limited displacement, along with a 10 to 45 times reduction in the permeability perpendicular to the shear zone with increasing normal stress. No change in shear mode occurred in the unweathered mudstone samples or weathered sandstone samples under the same wet conditions.

The particle microstructure with increasing pores in at the particle boundaries was sensitive to the water, which triggered mineral separation and mud generation and filling throughout the specimens. With the concomitant increment in particle roundness and uniformity, the mud resulted in the reduction in the shear resistance and permeability by lubricating the particle surfaces and sealing the micropores. Our experimental results contribute to revealing the rapid strength reduction of soft interlayers within limited amounts of shear displacement, which may be related to landslide initiation and shallow fault activation

during groundwater infiltration.

Acknowledgement

This research was supported by the National Natural Science Foundation of China (Grant Nos. 42090054, 41521002 and 41972284) and the National Key R&D Program of China (2017YFC1501301). This work was also supported by the research fund of the State Key Laboratory of Geohazard Prevention and Geoenvironment Protection (No. SKLGP2020Z005). Data sets for this research are available in a repository (https://figshare.com/%5bdoi: 10.6084/m9.figshare.14987853])

References:Agung, M.W., Sassa, K., Fukuoka, H. and Wang, G., 2004. Evolution of shear-zone structure in undrained ring-shear tests. Landslides, 1(2): 101-112.Alberti, S., Wang, G., Dattola, G. and Crosta, G.B., 2019. Physical mechanical characterization of a rockslide shear zone by standard and unconventional tests. Landslides, 16(4): 739-750.ASTM D 3080, 2001. Standard test method for direct shear test of soils under consolidated drained conditions. ASTM Standards on Disk, vol. 0.4-0.8.Chandler, R.J., 1969. The effect of weathering on the shear strength properties of Keuper marl. Geotechnique, 19(3): 321-334.Christaras, B., 1997. Landslides in iliolitic and marly formations. Examples from north-western Greece. Engineering Geology, 47(1-2): 57-69.Crawford, B.R., Faulkner, D.R. and Rutter, E.H., 2008. Strength, porosity, and permeability development during hydrostatic and shear loading of synthetic quartz-clay fault gouge. Journal of Geophysical Research-Solid Earth, 113(B3).Cuisiat, F. and Skurtveit, E., 2010. An experimental investigation of the development and permeability of clay smears along faults in uncemented sediments. Journal of Structural Geology, 32(11): 1850-1863.Dewhurst, D., Clennell, M., Brown, K. and Westbrook, G., 1996. Fabric and hydraulic conductivity of sheared clays. Geotechnique, 46(4): 761-768.Eberhardt, E., Thuro, K. and Luginbuehl, A., 2005. Slope instability mechanisms in dipping interbedded conglomerates and weathered marls - the 1999 Rufi landslide, Switzerland. Engineering Geology, 77(1-2): 35-56.Faoro, I., Niemeijer, A., Marone, C. and Elsworth, D., 2009. Influence of shear and deviatoric stress on the evolution of permeability in fractured rock. Journal of Geophysical Research-Solid Earth, 114(B1).Feia, S., Sulem, J., Canou, J., Ghabezloo, S. and Clain, X., 2016. Changes in permeability of sand during triaxial loading: effect of fine particles production. Acta Geotechnica, 11(1): 1-19.Fukuoka, H., Sassa, K. and Wang, G., 2007. Influence of shear speed and normal stress on the shear behavior and shear zone structure of granular materials in naturally drained ring shear tests. Landslides, 4(1): 63-74.Gokceoglu, C., Ulusay, R. and Sonmez, H., 2000. Factors affecting the durability of selected weak and clay-bearing rocks from Turkey, with particular

emphasis on the influence of the number of drying and wetting cycles. Engineering Geology, 57(3-4): 215-237.Ikari, M.J. and Saffer, D.M., 2012. Permeability contrasts between sheared and normally consolidated sediments in the Nankai accretionary prism. Marine Geology, 295: 1-13.Ikari, M.J., Saffer, D.M. and Marone, C., 2009. Frictional and hydrologic properties of clay-rich fault gouge. Journal of Geophysical Research-Solid Earth, 114.Kimura, S. et al., 2019. Water permeability evolution with faulting for unconsolidated turbidite sand in a gas-hydrate reservoir in the eastern Nankai trough area of Japan. Journal of Geophysical Research-Solid Earth, 124(12): 13415-13426.Kimura, S. et al., 2020. Experimental study of impact of shearing velocity and effective normal stress on post-shearing permeability evolution of silica fault gouges. Tectonophysics, 789: 228521.Kimura, S., Kaneko, H., Noda, S., Ito, T. and Minagawa, H., 2018. Shear-induced permeability reduction and shear-zone development of sand under high vertical stress. Engineering Geology, 238: 86-98.Li, W. et al., 2020. Deformation characteristics and failure mechanism of a reactivated landslide in Leidashi, Sichuan, China, on August 6, 2019: an emergency investigation report. Landslides, 17(6): 1405-1413.Liu, C., Shi, B., Zhou, J. and Tang, C., 2011. Quantification and characterization of microporosity by image processing, geometric measurement and statistical methods: Application on SEM images of clay materials. Applied Clay Science, 54(1): 97-106.Liu, X., Song, Y., Xia, Z. and Chen, R., 2020. Assessing the slake durability of red stratum sandstone in different solution environments by a novel dual rotation test. Engineering Geology, 267: 105503.Lupini, J.F., Skinner, A.E. and Vaughan, P.R., 1981. The drained residual strength of cohesive soils. Geotechnique, 31(2): 181-213.Ma, C., Zhan, H., Zhang, T. and Yao, W., 2019. Investigation on shear behavior of soft interlayers by ring shear tests. Engineering Geology, 254: 34-42.Mair, K., Frye, K. and Marone, C., 2002. Influence of grain characteristics on the friction of granular shear zones. Journal of Geophysical Research-Solid Earth, 107(B10).Morrow, C., Lockner, D.A. and Hickman, S., 2015. Low resistivity and permeability in actively deforming shear zones on the San Andreas. Journal of Geophysical Research-Solid Earth, 120(12): 8240-8258.Panek, T. et al., 2011. Rainfall-induced landslide event of May 2010 in the eastern part of the Czech Republic. Landslides, 8(4): 507-516.Reece, J.S., Flemings, P.B., Dugan, B., Long, H. and Germaine, J.T., 2012. Permeability-porosity relationships of shallow mudstones in the Ursa Basin, northern deepwater Gulf of Mexico. Journal of Geophysical Research-Solid Earth, 117: B12102.Riaz, S., Wang, G., Basharat, M. and Takara, K., 2019. Experimental investigation of a catastrophic landslide in northern Pakistan. Landslides, 16(10): 2017-2032.Schneider, J., Flemings, P.B., Day-Stirrat, R.J. and Germaine, J.T., 2011. Insights into pore-scale controls on mudstone permeability through resedimentation experiments. Geology, 39(11): 1011-1014.Tang, H. et al., 2015. Evolution characteristics of the Huangtupo landslide based on in situ tunneling and monitoring. Landslides, 12(3): 511-521.Tanikawa, W. et al., 2012. Velocity dependence of shear-induced permeability associated with frictional behavior in fault zones of the Nankai subduction zone. Journal of Geophysical Research-Solid Earth, 117: B05405.Uehara, S. and Takahashi, M., 2014. Evolution of permeability and

microstructure of experimentally-created shear zones in Neogene siliceous mudstones from Horonobe, Japan. Journal of Structural Geology, 60: 46-54.Xu, Q., Liu, H., Ran, J., Li, W. and Sun, X., 2016. Field monitoring of groundwater responses to heavy rainfalls and the early warning of the Kualiangzi landslide in Sichuan Basin, southwestern China. Landslides, 13(6): 1555-1570.Zhang, S., Tullis, T. and Scruggs, V., 1999. Permeability anisotropy and pressure dependency of permeability in experimentally sheared gouge materials. Journal of Structural Geology, 21(7): 795-806.Zhang, Z. and Gao, W., 2020. Effect of different test methods on the disintegration behaviour of soft rock and the evolution model of disintegration breakage under cyclic wetting and drying. Engineering Geology, 279: 105888.Zou, Z., Tang, H., Xiong, C., Su, A. and Criss, R., 2017. Kinetic characteristics of debris flows as exemplified by field investigations and discrete element simulation of the catastrophic Jiweishan rockslide, China. Geomorphology, 295: 1-15.